

Can MOND take a bullet? Analytical comparisons of three versions of MOND beyond spherical symmetry

G. W. Angus^{1*}, B. Famaey^{2†} and H. S. Zhao^{1‡}

¹*SUPA, School of Physics and Astronomy, University of St. Andrews, Scotland KY16 9SS*

²*Institut d'Astronomie et d'Astrophysique, Université Libre de Bruxelles, CP 226, Boulevard du Triomphe, B-1050 Bruxelles, Belgium*

Accepted ... Received ... ; in original form ...

ABSTRACT

A proper test of Modified Newtonian Dynamics (MOND) in systems of non-trivial geometries depends on modelling subtle differences in several versions of its postulated theories. This is especially important for lensing and dynamics of barely virialised galaxy clusters with typical gravity of scale $\sim a_0 \sim 1 \text{Ås}^{-2}$. The original MOND formula, the classical single field modification of the Poisson equation, and the multi-field general relativistic theory of Bekenstein (TeVeS) all lead to different predictions as we stray from spherical symmetry. In this paper, we study a class of analytical MONDian models for a system with a semi-Hernquist baryonic profile. After presenting the analytical distribution function of the baryons in spherical limits, we develop orbits and gravitational lensing of the models in non-spherical geometries. In particular, we can generate a multi-centred baryonic system with a weak lensing signal resembling that of the merging galaxy cluster 1E 0657-56 with a bullet-like light distribution. We finally present analytical scale-free highly non-spherical models to show the subtle differences between the single field classical MOND theory and the multi-field TeVeS theory.

Key words: gravitation - dark matter - galaxy: kinematics and dynamics, structure

1 INTRODUCTION

While luminous models for the central parts of galaxies do not usually require a dark matter (DM) component, massive halos of DM must be taken into account if one wants to construct realistic potential-density pairs for an entire galaxy, in order to reproduce the observed nearly-flat galactic rotation curves.

Curiously, there is a considerable body of evidence that the galactic mass profiles of baryonic and dark matter are not uncorrelated (McGaugh 2005). The correlation between the Newtonian gravity of the baryons \mathbf{g}_N and the overall gravity \mathbf{g} (baryons plus DM) can be loosely parameterized by Milgrom's (1983) empirical relation

$$\mu(g/a_0) \mathbf{g} = \mathbf{g}_N, \tag{1}$$

where the interpolating function $\mu(x)$ is a function which runs smoothly from $\mu(x) = x$ at $x \ll 1$ to $\mu(x) = 1$ at $x \gg 1$ with a dividing gravity scale $a_0 \sim 1 \text{Ås}^{-2}$ at the transition. It is a very serious challenge for cold dark matter simulations to reproduce this empirical relation. On the other hand, this relation can be interpreted as a modification of the Newton-Einstein gravitational law in the ultra-weak field regime, with no actual need for dark matter (at the galaxy scale). This provocative idea was taken as the basis for the MOND theory: however, using Eq.(1) alone to transform \mathbf{g}_N into \mathbf{g} does not provide a respectable gravitational force preserving energy and angular momentum.

Bekenstein & Milgrom (1984) then suggested modifying the Poisson Equation in order to produce a non-relativistic MOND potential. This proposal was recently refined by Bekenstein (2004) who presented a Lorentz-covariant theory of gravity, dubbed TeVeS, yielding MONDian behaviour in the appropriate limit. However, there is a subtle difference between the non-relativistic formulation of MOND and the relativistic TeVeS, namely the number of fields involved: in MOND, the potential is modified

* email: gwa2@st-andrews.ac.uk

† FNRS Scientific Collaborator; email: bfamaey@ulb.ac.be

‡ email: hz4@st-andrews.ac.uk

directly in order to trigger the MOND phenomenology, while in TeVeS, a scalar field is added to the traditional Newtonian potential. These two descriptions are equivalent only in highly symmetric systems (spherical or cylindrical symmetry). For disk galaxies, Eq.(1) is a good approximation of the MOND and TeVeS gravitational theories since the additional curl field (see §2) is small when solving the modified Poisson equation for the potential or the scalar field (Brada & Milgrom 1995). For this reason, Eq.(1) has been used with confidence to fit the rotation curves of an impressive list of external galaxies with remarkable accuracy (Sanders & McGaugh 2002). However, very little work has been carried out to study the actual effect of the curl field in the non-relativistic MOND theory (Brada & Milgrom 1995, 1999; Ciotti, Londrillo & Nipoti 2006), while the quantitative difference between the predictions of MOND and TeVeS has not been studied at all. The issue has become urgent as recent evidence against MOND is largely based on multi-centred systems such as satellites of the Milky Way (Zhao 2005) and the bullet cluster of merging galaxies (Clowe et al. 2004).

In this paper, after recalling some basic formulae of MOND and TeVeS (§2), we propose a set of parametric interpolating functions that are physical in TeVeS (§3). Then we present spherical analytical potential-density pairs for the baryon distribution in early type galaxies, galactic bulges and dwarf spheroidals, valid in MOND as well as in TeVeS (§4). For this model we work out the density, potential, circular velocity, isotropic and anisotropic distribution functions. We also show a simple analytical expression for the gravitational bending angle. Then we present the combination of such models in multi-centred systems for the classical MOND approximation (§5); this provides an indication of the kind of result we could expect from a rigorous modelling of the bullet cluster of galaxies (Clowe et al. 2004). More generally, we then show how to extend those spherical models to oblate ones (§6). In those non-spherical situations, the density corresponding to a given potential differs in the classical MOND and in TeVeS. To illustrate this, we study the effects of the flattening of the potential in the special case of scale-free oblate one-dimensional models (§7), and we explicitly show the subtle differences between the different theoretical frameworks. Note that Milgrom (1994) has also suggested that MOND could have a modified inertia basis rather than a modified gravity basis; in that case the original MOND formula is correct for circular orbits in galaxies, the theory would become strongly non-local, the conservation laws would become unusual, and the potential-density approach used hereafter would not apply to that framework.

2 MOND AND TEVES

In the quadratic Lagrangian theory of MOND by Bekenstein & Milgrom (1984), the Poisson equation reads

$$\nabla \cdot [\mu \nabla \Phi] = \nabla^2 \Phi_N = 4\pi G \rho, \quad (2)$$

where $\mu(|\nabla \Phi|/a_0)$ is the same interpolating function as in Eq.(1). We then have

$$\mu(g/a_0) \mathbf{g} = \mathbf{g}_N + \nabla \times \mathbf{H}. \quad (3)$$

The value of the curl field depends on the boundary conditions, but vanishes in spherical symmetry where Gauss' theorem applies and Eq.(1) is recovered. In realistic geometries, the curl field is non-zero but small (see Brada & Milgrom 1995, 1999; Ciotti et al. 2006), leading to small differences when computing the rotation curves of spiral galaxies.

On the other hand, Bekenstein's relativistic MOND (Bekenstein 2004) is a tensor-vector-scalar (TeVeS) theory: the tensor is an Einstein metric $g_{\alpha\beta}$ out of which is built the usual Einstein-Hilbert action. U_α is a dynamical normalized vector field ($g^{\alpha\beta} U_\alpha U_\beta = -1$), and ϕ is a dynamical scalar field. The action is the sum of the Einstein-Hilbert action for the tensor $g_{\alpha\beta}$, the matter action, the action of the vector field U_α , and the action of the scalar field ϕ . Einstein-like equations are obtained for each of these fields by varying the action w.r.t. each of them.

In TeVeS, the physical metric near a quasi-static galaxy is given by the same metric as in General Relativity, with the Newtonian potential Φ_N replaced by the total potential

$$\Phi = \Xi \Phi_N + \phi, \quad (4)$$

where $\Xi \simeq 1$. This means that the scalar field ϕ plays the role of the dark matter gravitational potential. The Einstein-like equation for the scalar field relates it to the Newtonian potential Φ_N (generated by the baryonic density ρ) through the equation

$$\nabla \cdot [\mu_s \nabla \phi] = \nabla^2 \Phi_N = 4\pi G \rho, \quad (5)$$

where μ_s is a function of the scalar field strength $g_s = |\nabla \phi|$, and derives from a free function in the action of the scalar field.

3 THE INTERPOLATING FUNCTIONS

In spherical symmetry, we have

$$\mu_s g_s = \mu(g_s + g_N) = g_N, \quad (6)$$

where μ is the interpolating function of MOND, thus related to μ_s by

$$\mu_s = \frac{\mu}{1 - \mu}. \quad (7)$$

The standard interpolating function that has been used for twenty years to fit the rotation curves with Eq.(1) is

$$\mu(x) = \frac{x}{\sqrt{1+x^2}}. \quad (8)$$

However, Zhao & Famaey (2006) have shown that this function, or rather the corresponding function μ_s derived from Eq.(7), is not physical in the framework of TeVeS; the function μ_s is multi-valued. For this reason, we will use hereafter a parametric set of interpolating functions that are physical in TeVeS:

$$\mu(x) = \frac{2x}{1 + (2-\alpha)x + \sqrt{(1-\alpha x)^2 + 4x}}, \quad 0 \leq \alpha \leq 1, \quad (9)$$

where $x = g/a_0$. The corresponding scalar field functions are

$$\mu_s(s) = \frac{s}{1-\alpha s}, \quad (10)$$

where $s = g_s/a_0$. The $\alpha = 0$ case corresponds to the toy model proposed by Bekenstein (2004) in weak and intermediate gravity. Under the approximation of Eq.(1), the $\alpha = 1$ model has been shown by Famaey & Binney (2005) and Zhao & Famaey (2006) to be a better fit to the rotation curves of galaxies than the $\alpha = 0$ case. The values $0 < \alpha < 1$ have not yet been explored in real galaxies, and will be the subject of another paper (Famaey, Gentile & Zhao 2006, in preparation).

These functions μ and μ_s will lead to the same gravitational behaviour in spherical symmetry. However, note that Eq.(7) is not valid in a more general geometry: the Newtonian force, the MOND force of Bekenstein & Milgrom (1984) and the TeVeS force are no longer parallel. The curl field obtained when solving the equation for the scalar field ϕ (Eq. 5) will be different than the one obtained when solving for the full Φ in Eq.(2). This will be illustrated in §7.

4 SPHERICAL POTENTIAL-DENSITY PAIRS IN MOND/TEVES

In this section, we consider only the $\alpha = 1$ case, known to yield excellent fits to the rotation curves of galaxies. Potential-density pairs (e.g., Hernquist 1990, Dehnen 1993, Zhao 1995) have long been acknowledged to be very useful in model building and in checking numerical simulations. It is even more interesting to find simple spherical and non-spherical models in MOND and TeVeS. We explore a spherical model with a scalar field of the form

$$\phi(r) = v_0^2 \ln \left(1 + \frac{r}{(p+1)r_0} \right), \quad (11)$$

where p is a dimensionless number, and

$$r_0 \equiv \frac{v_0^2}{a_0}, \quad v_0^2 = \sqrt{GM_0 a_0}. \quad (12)$$

Then we have, according to the equation for the scalar field (Eq. 5), that

$$\rho(r) = \frac{M_0 [r_h(r+r_h) - r_0^2/4]}{2\pi r [(r+r_h)^2 - r_0^2/4]^2}, \quad r_h = (p + \frac{1}{2})r_0 \quad (13)$$

The density profile is shown for $p=0.5$ and 2.0 in Fig.1. This MONDian density distribution is realistic: the model mimics the Sersic profile of an elliptical galaxy. It also mimics a Hernquist (1990) model with scalelength r_h :

$$\rho_h(r) = \frac{M_0 r_h}{2\pi r (r+r_h)^3}. \quad (14)$$

We can then also easily derive $g_s = v_0^2/(r+r_0+pr_0)$, and from Eq.(6) calculate the Newtonian and total potential of the model:

$$\Phi_N(r) = \Phi - \phi(r), \quad \Phi(r) = v_0^2 \ln \left(1 + \frac{r}{pr_0} \right). \quad (15)$$

Thus, for the gravity we have

$$g(r) = \frac{V_c^2}{r} = \frac{v_0^2}{r+pr_0}. \quad (16)$$

The corresponding matter density (baryons + DM) in the Newtonian framework is

$$\rho(r) + \rho_{DM}(r) = \frac{M_0(1 + \frac{2pr_0}{r})}{4\pi r_0(pr_0+r)^2}. \quad (17)$$

The asymptotic circular velocity is v_0 , and the maximum gravity g_0 occurs at small r (near the origin), where $g(r) = \frac{v_0^2}{pr_0} = \frac{a_0}{p}$ (note that in the flattened models of §7 g_0 will be related to p by $g_0 = \frac{a_0}{p}$). Given this, it is interesting to show the spherical model with $p=0.5$ and 2.0 , hence the intermediate gravity range $g_0 = 2a_0$ and $a_0/2$ (Figs. 1-4). Most bulges and ellipticals,

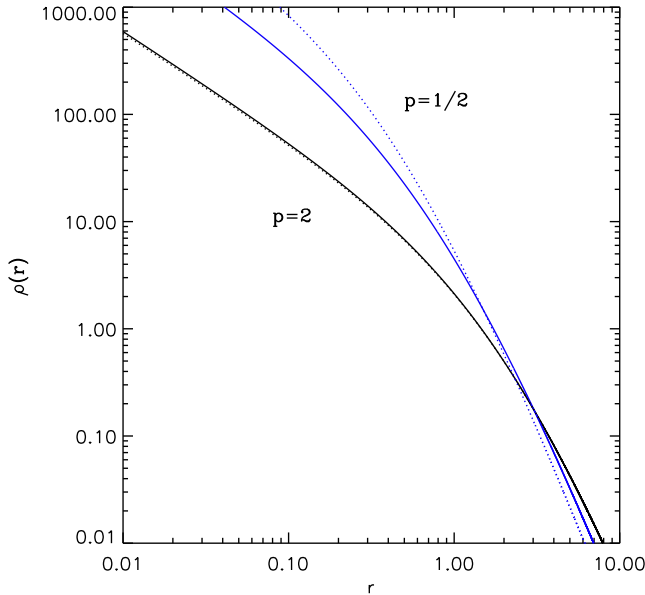


Figure 1. Shows the density of Eq.(13) for $p=0.5$ and 2.0 . r_0 and v_0^2 are taken to be unity, and $G=0.00442$ in all following plots unless stated otherwise. Overplotted is a Hernquist density profile (cf. Eq. 14) for $p=0.5$ and 2.0 . It shadows the curve for $p=2$ from our density profile extremely well, but there is a slight deviation between the $p=0.5$ curves.

gravitational lenses and galaxy clusters should go through this intermediate regime, while dwarf spheroidal galaxies have very low $g_0/a_0 = \frac{1}{p}$. Although a detailed fit to observed light profile is beyond the scope of the present paper, we will show an application in galaxy clusters in §5.

4.1 The baryonic distribution function

It is interesting to ask if the MONDian potential-density pairs presented in the previous section can be realised by some equilibrium configurations described by certain baryonic distribution functions self-consistently. This can be done in exactly the same way as in Newtonian gravity. This is particularly simple for a system with constant radial anisotropy such that the radial velocity dispersion σ_r is related to the tangential dispersions by $\sigma_r^2 = 2\sigma_\theta^2 = 2\sigma_\phi^2$. In this case the baryonic phase-space distribution F for the distribution function must take the form:

$$F(E, L) = \frac{A(E)}{4\pi L}, \quad A(E) \equiv -\left. \frac{d(r\rho)}{d\Phi} \right|_{\Phi=E}. \quad (18)$$

Knowing from Eq.(15) that

$$r(\Phi) = pr_0 \left(\exp \frac{\Phi}{v_0^2} - 1 \right), \quad (19)$$

we obtain

$$F(E, L) = \frac{M_0}{16\pi^2 r_0^2 v_0^2 L} \frac{\Lambda^3 (2\Lambda^2 + (6p+1)\Lambda + 3p(2p+1))}{p(p+\Lambda)^3}, \quad \Lambda = \exp \frac{-E}{v_0^2}. \quad (20)$$

For this radially anisotropic model we can calculate the radial velocity dispersion by solving the Jeans equation as done for Newtonian system (e.g., Angus & Zhao 2006)

$$2\sigma_\theta^2 = 2\sigma_\phi^2 = \sigma_r^2(r) = \frac{1}{r\rho} \int_r^\infty V_c^2 \rho dr. \quad (21)$$

Substitute in the expression for the circular velocity V_c we have

$$\sigma_r^2(r) = v_0^2 \frac{(s^2 - 1)^2}{4(2p+1)s - 4} \left[\left(\frac{p}{2} + 1 \right) \left(\ln \frac{s-1}{s+1} + \frac{2}{s+1} \right) + \frac{2}{s^2 - 1} + \frac{p}{(s-1)^2} \right] \quad (22)$$

where $s \equiv 1 + 2p + \frac{2r}{r_0}$. A likewise expression can be found by calculating the moments from the distribution function $F(E, L)$.

An interesting feature of this model is that it has *nearly isothermal* velocity dispersions everywhere for any value of the parameter p . Fig.(2) shows $\sigma_r(r)$ for the two limiting cases of $p = 0$ and $p = \infty$. To understand this note that at large

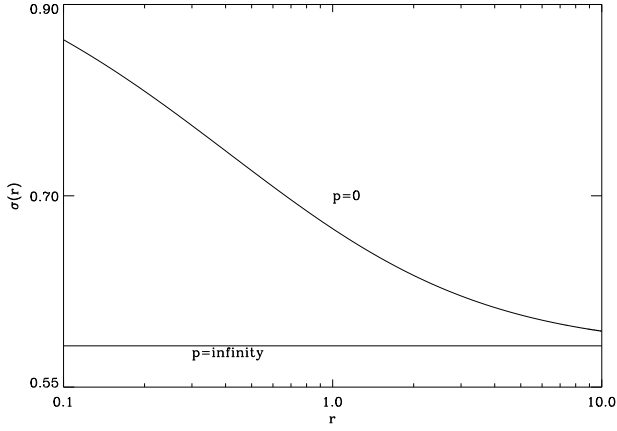


Figure 2. Shows the radial velocity dispersion of anisotropic model given by Eq.(22) for the limiting cases $p=0$ and $p=\infty$. Here v_0 and r_0 are unity.

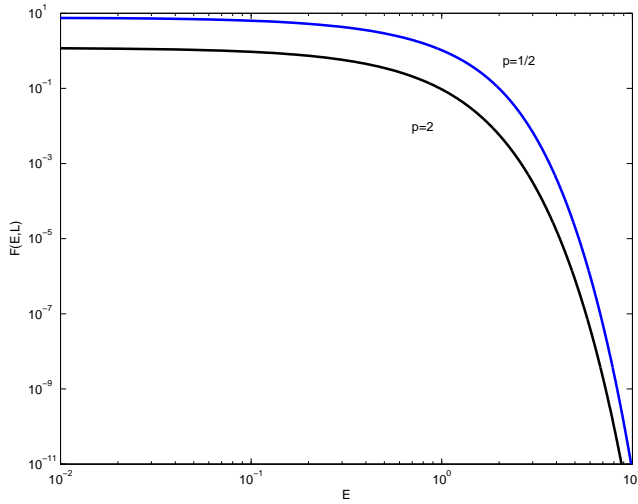


Figure 3. Shows the anisotropic distribution function from Eq.(20) at $L = 1$ for $p=0.5$ and 2.0

radii $\rho \sim r^{-4}$, $V_c \rightarrow v_0$ and $\sigma_r^2 \rightarrow \frac{v_0^2}{3}$. At small radii, $r\rho \rightarrow cst$, and $\sigma_r^2(0) = (p+1)v_0^2 \left[3/4 + p/2 + p(p/2+1) \ln \frac{p}{p+1} \right] = 0.75v_0^2, 0.470v_0^2, 0.421v_0^2, 0.383v_0^2, 0.333v_0^2$ for $p = 0, 0.5, 1, 2, \infty$. So for all plausible values of p , σ_r^2 is very comparable at the center and at large radii. The anisotropic distribution function as a function of E is presented in Fig.(3) for $p = 0.5$ and $p = 2.0$. We can also numerically integrate the isotropic distribution function via Eddington's equation (see appendix and Fig.4).

4.2 Gravitational lensing

Light bending in TeVeS works very much like in General Relativity. For a ray of impact parameter R from the spherical lens, the bending angle θ is given (cf. Zhao, Bacon, Taylor, Horne 2006) by the following integration along the line of sight

$$\theta(R) = \int_{-\infty}^{+\infty} \frac{2g_{\perp} dz}{c^2}, \quad g_{\perp}(R, z) = g(r) \frac{R}{r}, \quad (23)$$

where $g_{\perp}(R, z)$ is the gravity perpendicular to the line of sight, and $g(r)$ is the centripetal gravity at radius $r = \sqrt{R^2 + z^2}$. Using the expression for $g(r)$ from our model (Eq. 16), we find that the deflection angle is given by

$$\theta(R) = \begin{cases} \frac{8v_0^2}{c^2 \sqrt{1-y^{-2}}} \arctan \sqrt{\frac{y-1}{y+1}} & \text{when } y \equiv \frac{R}{pr_0} > 1 \\ \frac{4v_0^2}{c^2} & \text{when } y \equiv \frac{R}{pr_0} = 1 \\ \frac{8v_0^2}{c^2 \sqrt{y^{-2}-1}} \tanh^{-1} \sqrt{\frac{1-y}{y+1}} & \text{when } y \equiv \frac{R}{pr_0} < 1 \end{cases} \quad (24)$$

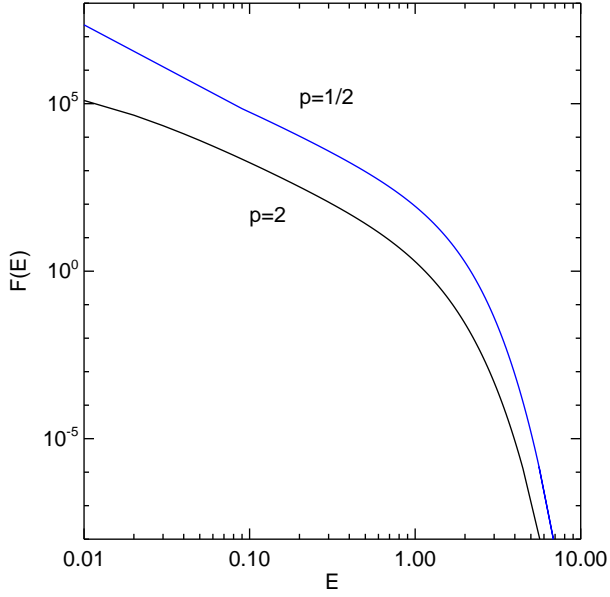


Figure 4. Shows the isotropic distribution function derived in the appendix for $p=0.5$ and 2.0 .

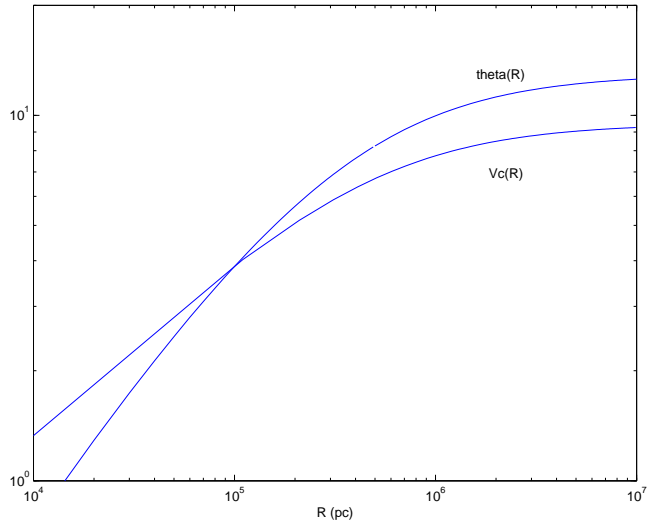


Figure 5. Shows the bending angle θ in arcseconds as a function of impact parameter R and the circular speed V_c in 10^2 km s^{-1} for $pr_0=0.5 \text{ Mpc}$ and $v_0=949 \text{ km s}^{-1}$.

Fig.5 shows the predicted bending angle as function of the impact parameter R ; cases are shown for $p = 0.5$ and 2.0 . The bending angle increases with the impact parameter and starts to level off beyond $R = pr_0$. This is consistent with the expectation of a flat rotation curve at large radii (Fig. 5). Given the distance to the lens D_l , the distance to the source D_s and the lens-source distance D_{ls} we can define an effective distance as $D_{\text{eff}} = D_l D_{ls} / D_s$. Using this we can compute the convergence κ and the tangential shear γ from

$$\begin{aligned}
 \kappa(R) &= \frac{\theta D_{\text{eff}}}{R} - \gamma(R) \\
 &= \frac{R^2 - 2(pr_0)^2}{2R^2 - 2(pr_0)^2} \frac{(\theta - \theta(pr_0)) D_{\text{eff}}}{R},
 \end{aligned} \tag{25}$$

and they are plotted for a toy cluster in Fig.(6).

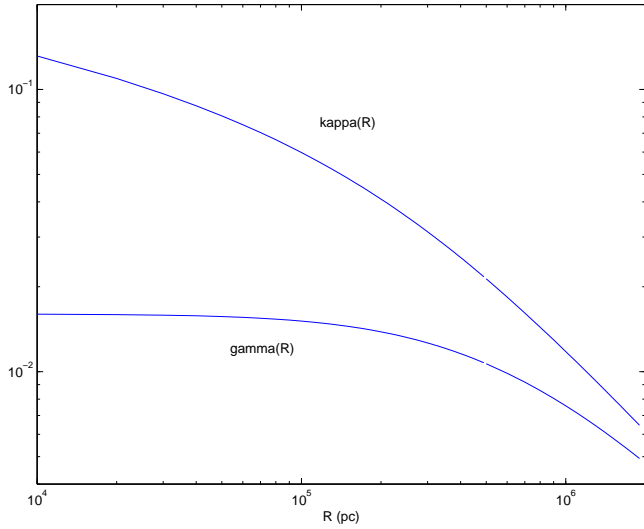


Figure 6. Shows the convergence κ and tangential shear γ for a toy cluster at an effective distance $D_{\text{eff}}=400\text{Mpc}$ with $v_0=949\text{ km s}^{-1}$ and $pr_0=0.5\text{Mpc}$.

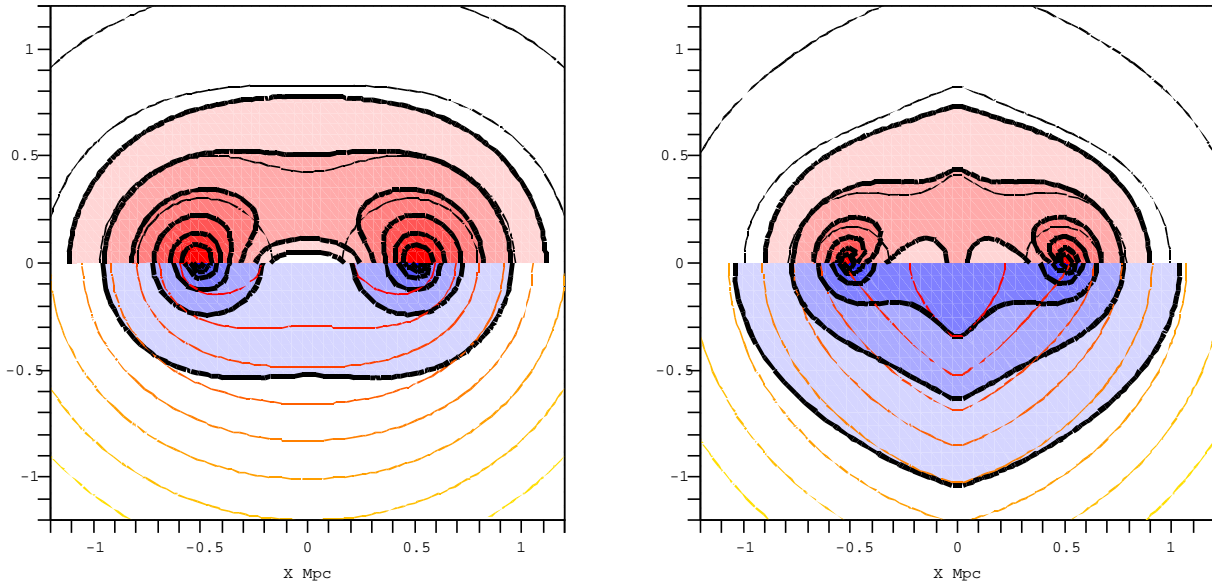


Figure 7. Shows contours of a double-centred (panel a) and a triple-centred (panel b) analytical model for the potential Φ (dashed red lower) and projected lensing convergence κ (thick blue shaded lower) of a system resembling the bullet cluster (Clowe et al. 2004). Also shown are contours (spaced in 0.5 dex, in intervals of factor of two) the matter volume density in Einstein-Newton gravity (upper thin black) and baryonic matter volume density in the classical MOND approximation (upper shaded zones). Note a density minimum for 'MONDian' baryons at $(0,0)$ in panel (a), and a density maximum in panel (b) where the baryons are primarily in a disk component in the middle.

5 MULTI-CENTRED POTENTIALS AND THE MERGING BULLET CLUSTER

An obvious way of obtaining flattened models is to consider a double-centred potential, whose axis of symmetry is perpendicular to the line of sight, i.e., a merging system viewed edge-on. In a cartesian coordinate system (x, y, z) , if the two centres are located at $(-x_0, 0, 0)$ and $(x_0, 0, 0)$, then the double-centred potential can be written as

$$\Phi_{\text{dc}}(x, y, z) = \frac{\Phi(r_1)}{2} + \frac{\Phi(r_2)}{2}, \quad (26)$$

where $r_1 = \sqrt{(x+x_0)^2 + y^2 + z^2}$, $r_2 = \sqrt{(x-x_0)^2 + y^2 + z^2}$, and Φ is the spherical potential of Eq.(16). Here we have simply added two spherical analytical potentials. For example, to mimic a merging galaxy cluster we set $p = 2$, $x_0 = pr_0 = 0.5\text{Mpc}$, $v_0 = 949\text{ km/s}$, and $M_0 = 5.21 \times 10^{13} M_\odot$.

The gravitational field of such a model is easily computed by the simple superposition of two spherical fields, i.e.,

$$\mathbf{g} = -\frac{v_0^2}{r_1 + pr_0} \frac{\mathbf{r}_1}{2r_1} - \frac{v_0^2}{r_2 + pr_0} \frac{\mathbf{r}_2}{2r_2}. \quad (27)$$

Likewise the light bending angle vector is the superposition of the bending angle vectors of two spherical models, so its x and y direction components are respectively

$$\begin{cases} \theta_{dcx}(x, y) = \frac{(x+x_0)\theta(R_1)}{2R_1} + \frac{(x-x_0)\theta(R_2)}{2R_2} \\ \theta_{dcy}(x, y) = \frac{y\theta(R_1)}{2R_1} + \frac{y\theta(R_2)}{2R_2}, \end{cases} \quad (28)$$

where $R_1 = \sqrt{(x+x_0)^2 + y^2}$, $R_2 = \sqrt{(x-x_0)^2 + y^2}$, and θ is the spherical bending angle of Eq.(24). From there we can estimate the projected lensing convergence

$$\kappa(x, y) = \frac{1}{2} D_{\text{eff}} \left(\frac{\partial \theta_{dcx}}{\partial x} + \frac{\partial \theta_{dcy}}{\partial y} \right) = \frac{\kappa(R_1)}{2} + \frac{\kappa(R_2)}{2}, \quad (29)$$

where $\kappa(R)$ is given by Eq.(25) for spherical systems. Assuming $D_{\text{eff}} = 400\text{Mpc}$, the resulting convergence contours are plotted on Fig. 7(a). This map resembles the convergence map derived from the weak lensing shear field around the merging bullet cluster 1E 0657+56 (Clowe et al. 2004).

So far the result does not differ from Einsteinian gravity. The difference is in the underlying matter distribution. In Einsteinian gravity, the convergence map is simply proportional to the surface density map, and the volume density of matter is the simple addition of two spherical models each with density given in Eq.(17). As we can see from Fig.7 there is a one-to-one relation between features in the convergence map and the features in the matter (dark plus baryons) distribution if the gravity is Einsteinian, i.e., what we see in lensing is what we have.

The situation in MOND/TeVeS is different. In order to properly derive the corresponding density in TeVeS, one would need to know what part of the double-centred potential is due to the scalar field. This will be done in the limiting case of scale-free flattened models in §7. Here we use the classical MOND approximation. From the gravity or the potential we can then directly calculate the corresponding baryonic isodensity contours using Eq.(2) and Eq.(9) with $\alpha = 1$. The MONDian baryonic matter has a rich structure. Fig.7(a) shows that at the centre ($x = 0, y = 0$) the MONDian volume density reaches a local minimum while the convergence map shows a saddle point. This cautions against a naive deprojection of the convergence map in MOND/TeVeS.

5.1 Triple-centred baryonic system and the bullet cluster 1E 0657+56

In the case of the bullet cluster, there are three baryonic mass concentrations. Clowe et al. (2004) argue that the bulk of baryonic mass is in the form of X-ray gas, which is shocked and displaced from the two optical centres of the colliding binary cluster. It was argued that lensing in any MONDian theory should produce shear maps centred on the dominating X-ray gas instead of the lesser baryonic mass responsible for the optical light. The fact that the convergence map coincides with the two optical centres is presented as direct evidence for the presence of collisionless dark matter, unaffected by the shock, and respecting the optical centres.

Of course, this is not so surprising since it is well known that MOND still needs an unseen matter component in galaxy clusters (Sanders 2003). But, in the case of the bullet, a key element of the line of reasoning is that the geometry of the lensing map in TeVeS reflects the underlying baryons even in highly non-spherical geometries. To illustrate the range of possibilities in triple-centred systems, let us consider the following potential

$$\Phi_{tc}(x, y, z) = [k_1 + (1 - k_1 - k_2)H(x)] \Phi(r_1) + [k_2 + (1 - k_1 - k_2)H(-x)] \Phi(r_2). \quad (30)$$

The terms involving the Heaviside-function create the effect of a razor thin disk at $x = 0$ (reminiscent of the well-known Kuzmin disk), with a sudden change of gravity in the x -direction at the midplane $x = 0$. The potential is continuous across the $x = 0$ plane. The deflection angle and convergence map remain those of the superposition of two spherical deflectors, although there is now a sudden change in the weighting of the two deflectors as one crosses the midplane $x = 0$. Finally one can apply the MONDian Poisson equation (Eq. 2) to derive the baryonic density.

Here we choose $k_1 = k_2 = 0.2$ so that we have a prominent baryonic component in between the two cluster centres. Fig.7(b) shows a rather regular looking convergence map, but a complex MONDian baryonic density distribution, somewhat resembling that of the bullet cluster. In particular, there is now a ridge of matter centred on $x = 0$ and two *irregular* baryonic components more or less centred on the $x = \pm x_0$. This example provides evidence that a regular-looking convergence map is not incompatible with a MONDian multi-centred baryonic mass distribution.

As argued in Zhao, Bacon, Taylor & Horne (2006) and Zhao & Qin (2006) the convergence κ can be *non-zero* where there is no projected matter in MOND/TeVeS, something that is not possible in Einsteinian gravity. This implies that a lensing convergence map does not simply translate a baryonic surface density map in MOND. Our models here show the range of non-trivial baryonic geometries for multi-centred potentials in MOND. Although the models here are of only indicative value

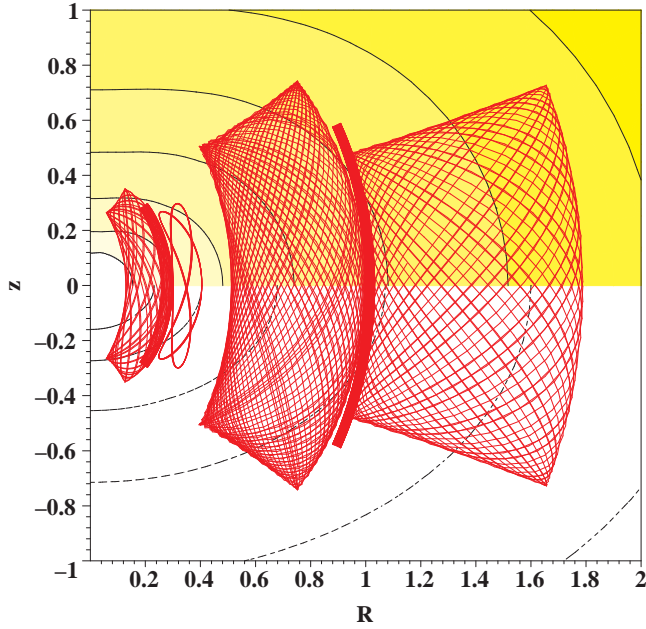


Figure 8. Shows a flattened non-scale-free potential with $g_0 = a_0/2$ ($p=2$), $\epsilon=0.25$, upper panel shading showing density contours (for $\alpha = 1$), bottom dashed showing Hernquist density profile (cf. Eq. 14) with axis ratio 2/3.

(as the approximation of classical MOND has been used, see §7 for typical differences with TeVeS) it does caution drawing conclusions about TeVeS before performing a careful lensing analysis of the bullet cluster (Clowe et al. 2004) in the framework of TeVeS.

6 FLATTENED POTENTIALS AND ORBITS

The spherical potential of §4 can also be generalised into a flattened or triaxial potential. For example, we can consider a model with an axisymmetric potential

$$\Phi(r, \theta) = \frac{v_0^2}{2} \ln \left[\left(1 + \frac{r}{pr_0} \right)^2 + 2\epsilon \frac{r}{pr_0} \cos^2 \theta \right] \quad (31)$$

where θ is the angle with the z -axis: $\epsilon > 0$ corresponds to an oblate potential and $\epsilon < 0$ to a prolate potential.

The corresponding density in the classical MOND of Bekenstein & Milgrom (1984) can be calculated by feeding this potential into the modified Poisson equation (Eq. 2) in spherical coordinates:

$$4\pi G\rho(r, \theta) = \frac{\partial}{r^2 \partial r} \frac{\mu \partial \Phi}{\partial r} + \frac{\partial}{r^2 \sin \theta \partial \theta} \frac{\mu \sin \theta \partial \Phi}{\partial \theta}. \quad (32)$$

The expression for ρ can be obtained analytically, but the general expression is too tedious to be given here. Nevertheless we can calculate orbits in this potential numerically. The stars in this flattened MOND potential are typically on loop orbits as in a flattened Newtonian potential (Fig. 8). We shall concentrate hereafter on a limiting case of this flattened model, in order to compare the predictions of the classical MOND gravity and of TeVeS.

7 SCALE-FREE FLATTENED MODELS: MULTI-FIELD THEORY VS. ONE-FIELD THEORY

In the limit $r/pr_0 \rightarrow 0$, the previous potential reduces to a scale-free form when expanding Eq.(31). We shall now consider such models with a total potential

$$\Phi(r, \theta) = rg_r(\cos \theta), \quad \text{where } g_r(c) = (1 + \epsilon c^2)g_0, \quad (33)$$

and for convenience we define

$$c \equiv \cos \theta. \quad (34)$$

Clearly, $g_0 = v_0^2/pr_0$ is thus the gravity along the major axis in the $c = 0$ (or $\theta = \pi/2$) plane, and the parameter ϵ leads to flattening ($\epsilon = 0$ reduces to the spherical case). The parameter g_0 is NOT the acceleration constant a_0 of MOND, but is a parameter of the model linked to it through the definitions (see Eq. 12) of v_0 and r_0 ($g_0 = a_0/p$).

This class of scale-free models corresponds to flattened galactic bulges, ellipticals, dwarf spheroidal galaxies, or centre of galaxy clusters depending on the value of the equatorial gravity g_0 . The radius-independent gravitational force in these models is:

$$\mathbf{g}(c) = \nabla\Phi(r, \theta) = g_r(c)\hat{r} + g_\theta(c)\hat{\theta}, \quad (35)$$

$$\text{where } g_\theta(c) = (1 - c^2)^{1/2} \left(\frac{dg_r}{dc} \right) = 2c\epsilon g_0(1 - c^2)^{1/2}. \quad (36)$$

The amplitude of gravity g is defined as

$$g(c) = [g_r(c)^2 + g_\theta(c)^2]^{1/2}. \quad (37)$$

We are now going to explore *the density corresponding to this potential in four different frameworks*: (i) Newtonian gravity where the computed density corresponds to the baryonic and DM distribution, (ii) classical one-field MOND gravity (Bekenstein & Milgrom 1984, approximation used in §5), (iii) TeVeS multi-field theory, (iv) original MOND formula (Eq. 1) approximation.¹

For the first time in the literature, we provide here a quantitative comparison of the three ways of describing the MOND phenomenology without invoking DM (and of Newtonian gravity with DM), by comparing the underlying density corresponding to the potential of Eq.(33).

7.1 Newtonian gravity with dark matter

Assuming Newtonian gravity, the density (corresponding to the stellar and dark densities) is

$$\rho(r, \theta) = (4\pi G)^{-1} \nabla^2 \Phi(r, \theta) = (4\pi G r)^{-1} L(c), \quad (38)$$

$$\text{where } L(c) = 2g_r(c) + \frac{d}{dc}[(1 - c^2)g'_r(c)] = \mathcal{L}[g_r(c)] = 2(1 + \epsilon)g_0 - 4\epsilon g_0 c^2, \quad (39)$$

We have defined the differential operator $\mathcal{L} = 2 + \frac{d}{dc}(1 + c^2)\frac{d}{dc}$. This toy model has a r^{-1} cusp, a rising rotation curve $V \propto \sqrt{r}$, and $M(r) \propto r^2$ (similar to uniform disks).

7.2 One-field MOND gravity

Now, assuming a classical MOND gravity (as we did in §5) with an interpolating function $\mu(g)$, the underlying (purely baryonic) density can be computed from

$$\rho_M(r, \theta) = (4\pi G)^{-1} \nabla \cdot (\mu \nabla \Phi(r, \theta)) = (4\pi G r)^{-1} L_M(c), \quad (40)$$

$$\text{where } L_M(c) = \mu(g)L(c) + (1 - c^2) \frac{d\mu(g)}{dc} \frac{dg_r}{dc}, \quad (41)$$

where $L(c)$ is given by Eq.(39) and $\mu(g)$ by Eq.(9) with g as in Eq.(37). This baryonic density $\rho_M(r, \theta)$ is compared with the baryonic+DM density of a Newtonian model with the same potential in Fig.9, for different values of g_0 and different interpolating functions.

7.3 Multi-field TeVeS gravity

To compute the baryonic density in §5 when making a toy model of the bullet cluster, we used the one-field MOND gravity. We are now going to show the differences that could be expected when using the multi-field TeVeS instead. The problem in that case is that we must find the relative contribution of the scalar field and of the Newtonian potential to the total potential before computing the underlying baryonic density.

Assuming a multi-field gravity (see Eqs. 4 and 5) with a scalar field ϕ and a Newtonian potential $\Phi_N = \Phi - \phi$, we have that the scalar field can be written in the form

$$\phi(r, \theta) = r g_{s,r}(\cos \theta), \text{ where } g_{s,r}(c) = g_r(c) - g_{n,r}(c) = g_0(1 + \epsilon c^2) - g_{n,r}(c), \quad (42)$$

where $g_{n,r}$ and $g_{s,r}$ are respectively the Newtonian gravity in the \hat{r} direction and the scalar field strength in the \hat{r} direction, both generated by the common density distribution we are looking for, $\rho_s(r, \theta)$.

The total scalar field strength is

$$g_s(c) = |\nabla\phi(r, \theta)| = (g_{s,r}^2(c) + g_{s,\theta}^2(c))^{1/2}, \text{ where } g_{s,\theta} = (1 - c^2)^{1/2} \left(\frac{dg_{s,r}}{dc} \right). \quad (43)$$

¹ In a flattened system, Eq.(1) does not derive from a proper theory of gravity (energy is generally not conserved). The only way to precisely recover it is to consider purely circular orbits in axisymmetric systems for non-relativistic modified inertia toy models (see Milgrom 1994). In a flattened system, the corresponding formula for the classical one-field MOND gravity will differ from Eq.(1) by a curl-field term (Eq. 3), while this curl-field will only affect the scalar field in TeVeS.

Table 1. Shows the correction to the rotation curve due to the curl field for six α 's (cf. Eq. 9) and for three representative gravity strengths ($g_0 = a_0/2$, a_0 and $2a_0$). $\epsilon = 0.8$.

$g_0 \rightarrow$	$a_0/2$			a_0			$2a_0$		
$\alpha \downarrow$	Δ_s	Δ_M	$\Delta_s - \Delta_M$	Δ_s	Δ_M	$\Delta_s - \Delta_M$	Δ_s	Δ_M	$\Delta_s - \Delta_M$
0.0	0.889	-0.782	1.671	-0.562	0.537	-1.100	-0.307	-0.223	-0.084
0.2	-0.044	-0.032	-0.011	0.525	-1.130	1.654	-0.648	1.375	-2.024
0.4	3.001	-1.627	4.628	-0.197	-0.123	-0.073	-0.807	5.808	-6.616
0.6	1.002	-0.895	1.898	-0.564	1.167	-1.731	-0.608	-0.334	-0.274
0.8	0.002	0.002	0.000	0.007	-1.238	1.244	-0.731	-7.074	6.343
1.0	-0.114	-1.985	1.871	-0.255	-0.102	-0.152	-0.820	-2.132	1.311

The baryon density is then given by both the scalar and Newtonian Poisson equations:

$$\rho_s(r, \theta) = (4\pi Gr)^{-1} \left\{ \mu_s \mathcal{L}[g_{s,r}(c)] + (1 - c^2) \frac{d\mu_s(g_s)}{dc} \frac{dg_{s,r}}{dc} \right\}, \quad (44)$$

and

$$\rho_s(r, \theta) = (4\pi Gr)^{-1} \mathcal{L}[g_r(c) - g_{s,r}(c)] \quad (45)$$

Combining the above two equations, we use the numerical relaxation method to solve the following second-order ODE for $g_{s,r}(c)$:

$$[1 + \mu_s] \mathcal{L}[g_{s,r}(c)] + (1 - c^2) \frac{d\mu_s(g_s)}{dc} \frac{dg_{s,r}}{dc} = L(c). \quad (46)$$

We set the boundary conditions such that the solution is regular at $c = \pm 1$. From this we derive the baryonic density $\rho_s(r, \theta)$.

We plot the equal density contours predicted from the three theories for a model with $g_0 = a_0/2$ and $2a_0$, $\alpha=0.0$ and 1.0 and $\epsilon=0.8$ in Fig.9. Note that some of the models have an unphysical heart-shaped density distribution. This doesn't prevent us comparing them in order to show the differences between the different formulations of MONDian modified gravity theories.

7.4 MOND formula approximation

In the case of the multi-field TeVeS gravity, if one subtracts the true gravity g_0 in the equatorial plane from the one that we would derive when applying Eq.(1) to the Newton-Einstein gravity, we obtain the correction to the rotation curve due to the curl field:

$$\Delta_s = \frac{g_{s,r}(0) \left(1 + \frac{g_{s,r}(0)}{1 - \alpha g_{s,r}(0)} \right) - g_0}{g_0}. \quad (47)$$

When this number is negative, the true MOND force is larger than the one derived using Eq.(1), while the opposite is true when this number is positive.

In the case of the one-field MOND gravity, the actual Newtonian gravitational force $g_N(c)$ can be calculated by solving the Newtonian Poisson equation for the density $\rho_M(r, \theta)$. Then, replacing $g_{s,r}(0)$ by $g_0 - g_N(0)$ in Eq.(47) yields Δ_M , the correction to the rotation curve due to the curl field in the non-relativistic MOND. Although the two values do not correspond to the same mass density, the relatively large values of the difference imply non-negligible differences. Those values are listed in Table 1 for three different values of g_0 ($a_0/2$, a_0 , $2a_0$), corresponding to the intermediate gravity regime, and for many different interpolating functions. We thus showed that it is necessary to do rigorous calculations using the scalar field prescription if one wants to address the intermediate regime quantitatively in complex geometries.

8 CONCLUSION

In summary, we have presented analytical models of dynamics and lensing in MOND/TeVeS.

1. We proposed (§3) a useful set of interpolating functions for MOND, with a physical counterpart in TeVeS, contrary to the standard interpolating function commonly used to fit galactic rotation curves.
2. Using our interpolating functions, we found a useful family of spherical (§4) models in MOND/TeVeS, with moderate $1/r$ cusps. Those models were then extended to non-spherical ones, by considering multi-centred models (§5), flattened models (§6) and scale-free flattened models (§7).

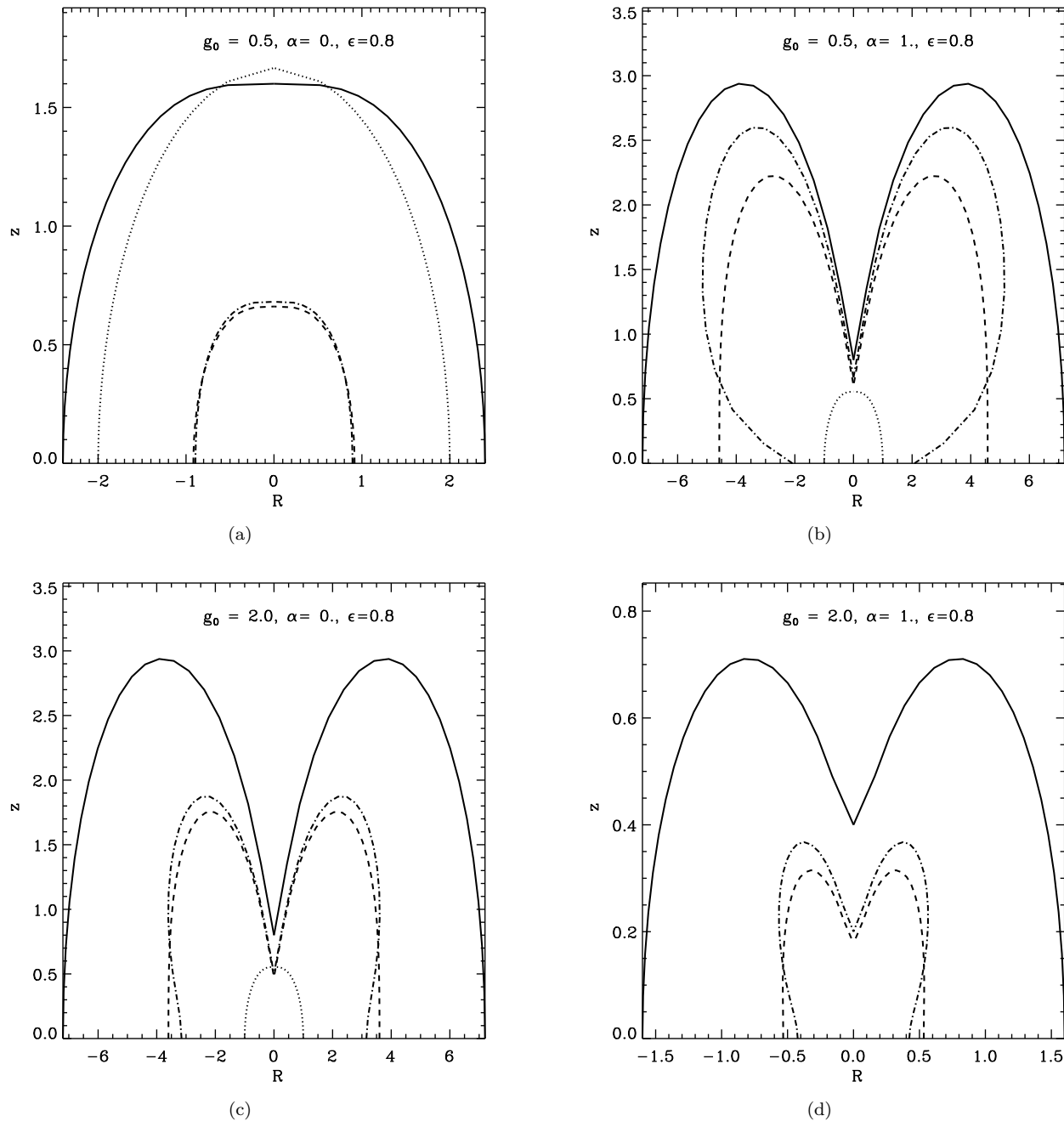


Figure 9. Shows isopotentials (dotted line) for the potential of Eq.(33), for 2 values of the equatorial gravity g_0 ($g_0 = a_0/2$ and $g_0 = 2a_0$), and 2 values of α (see Eq.(9)). The full black line corresponds to isodensity contours in Newtonian gravity (baryons+DM). The dashed line corresponds to baryonic isodensities for the one-field MOND and the dot-dashed line to the baryonic isodensities for the multi-field TeVeS. For the same potential, the typical density in TeVeS is slightly higher than in MOND near the centre, and slightly lower in the outskirts.

3. We showed that the lensing and the orbits in these spherical or flattened models are rather similar to the expectation in Einstein-Newton gravity, but still trigger a few surprises in extreme geometries. In multi-centred models, the convergence map does not always reflect the projected matter in the lens plane in MOND. This cautions simple interpretations of the analysis of weak lensing in the bullet cluster 1E 0657-56 (Clowe et al. 2004, see Fig. 7).

4. In flattened scale-free models (§7) we also found that there are differences in the potential-density pairs between the single-field MOND formulation of Bekenstein & Milgrom (1984) and the multi-field TeVeS formulation (Bekenstein 2004). However, the differences are probably not sufficient to solve the MONDian mass discrepancy in galaxy clusters (Sanders 2003) as suggested by Bekenstein (2005), unless other parameters of the TeVeS theory, e.g., Ξ (see Eq. 4), are important.

Note that our results are not inconsistent with the well-known result that rotation curves of astronomical disks are insensitive to the detailed formulation of MOND. While the very squashed axisymmetric systems of §7 are not very realistic by themselves, they seem to suggest that the three versions of MOND are likely to show greater differences in systems of complex multi-centred geometry, which is realistic for systems undergoing mergers.² Altogether we would argue that the most promising systems to test different versions of MOND are systems of lower symmetry for which MOND was not designed and the least is known. We have shown here that application of this test requires highly non-trivial computation to be done *properly*.

REFERENCES

- Angus G.W., Zhao H.S., 2006, submitted MNRAS
 Bekenstein J., 2004, Phys. Rev. D., 70, 3509
 Bekenstein J., 2005, astro-ph/0412652
 Bekenstein J., Milgrom M., 1984, ApJ, 286, 7
 Binney J., Tremaine, S., 1987, Galactic Dynamics (Princeton: Princeton University Press)
 Brada R., Milgrom M., 1995, MNRAS, 276, 453
 Brada R., Milgrom M., 1999, ApJ, 519, 590
 Ciotti L., Londrillo P., Nipoti C., 2006, ApJ, 640, 741
 Clowe D., Gonzalez A., Markevitch M., 2004, ApJ, 604, 596
 Dehnen W., 1993, MNRAS, 265, 250
 Famaey B., Gentile G., & Zhao H.S. 2006, in prep.
 Famaey B., Binney J., 2005, MNRAS, 363, 603
 Hernquist L., 1990, ApJ, 356, 359
 McGaugh S.S., 2005 Phys. Rev. Lett., 95, 171302
 Milgrom M., 1983, ApJ, 270, 365
 Milgrom M., 1994, Ann. Phys., 229, 384
 Sanders R.H., McGaugh S.S., 2002, ARA&A, 40, 263
 Sanders R.H., 2003, MNRAS, 342, 901
 Zhao H.S., 1997, MNRAS, 287, 525
 Zhao H.S., Famaey B., 2006, ApJ, 638, L9
 Zhao H.S., Bacon D., Taylor A.N., Horne K.D., 2006, MNRAS, 368, 171
 Zhao H.S., Tian L.L., 2006, A&A, 450, 1005
 Zhao H.S., 2005, A&A, 444, L25
 Zhao H.S., Qin B., 2006, ChJAA, 6, 141

APPENDIX A: ISOTROPIC DISTRIBUTION FUNCTION

Here we present the full isotropic distribution function corresponding to the models of §4. We start from the Eddington's formula (see Binney & Tremaine 1987)

$$F(E) = \frac{1}{\sqrt{8\pi^2}} \left[\int_E^\infty \frac{d^2\rho}{d\Phi^2} \frac{d\Phi}{\sqrt{\Phi - E}} + \frac{1}{\sqrt{\Phi - E}} \left(\frac{d\rho}{d\Phi} \right)_{\Phi=\infty} \right]. \quad (\text{A1})$$

Initially we define ρ as a function of Φ

$$\rho(\Phi) = \frac{M_0 \lambda^2 ((2p+1)\lambda^{-1} + 1)}{4\pi p^2 r_0^3 (\lambda^{-1} - 1)(p\lambda^{-1} + 1)^2}, \quad \lambda = \exp \frac{-\Phi}{v_0^2}. \quad (\text{A2})$$

The first derivative of ρ w.r.t. Φ is

$$\frac{2\pi r_0^3 v_0^2}{M_0} \frac{d\rho}{d\Phi} = \frac{-2p(2p+1)\lambda^{-1} + (3p^2 - 3p - 1) + (3p-1)\lambda + \lambda^2}{(\lambda^{-1} - 1)^2 (p\lambda^{-1} + 1)^3}. \quad (\text{A3})$$

Evaluated at $\Phi = \infty$ we get $\frac{d\rho}{d\Phi}|_{\Phi=\infty} = 0$. The second derivative w.r.t. Φ is

$$\frac{2\pi v_0^4 r_0^3}{M_0} \frac{d^2\rho}{d\Phi^2} = \frac{8p^2(2p+1)\lambda^{-3} + p(-23p^2 + 15p + 7)\lambda^{-2} + (9p^3 - 29p^2 + 11p + 2)\lambda^{-1} + (12p^2 - 20p + 3) + (8p - 5)\lambda + 2\lambda^2}{p^2(\lambda^{-1} - 1)^3 (p\lambda^{-1} + 1)^4}. \quad (\text{A4})$$

The reduced Eddington's formula

² For example, satellites in the tidal field of a galaxy have interesting Roche lobe shapes, which contain detailed information on the different laws of gravity (Zhao & Tian, 2006).

$$F(E) = \frac{1}{\sqrt{8\pi^2}} \left[\int_E^\infty \frac{d^2\rho}{d\Phi^2} \frac{d\Phi}{\sqrt{\Phi-E}} \right]. \quad (\text{A5})$$

can now easily be numerically integrated as shown in Fig.(4). This paper has been typeset from a $\text{T}_{\text{E}}\text{X}/\text{L}^{\text{A}}\text{T}_{\text{E}}\text{X}$ file prepared by the author.